Dynamic Image Data Compression in Spatial and Temporal Domains: Theory and Algorithm

Dino Ho, Dagan Feng, *Senior Member, IEEE,* and Kewei Chen

***Abstract*—Advanced medical imaging requires storage of large quantities of digitized clinical data. These data must be stored in such a way that their retrieval does not impair the clinician's ability to make a diagnosis. In this paper, we propose the theory and algorithm for near (or diagnostically) lossless dynamic image data compression. Taking advantage of domain-specific knowledge related to medical imaging, the medical practice and the dynamic imaging modality, a compression ratio greater than 80 : 1 is achieved. The high compression ratios are achieved by the proposed compression algorithm through three stages: 1) addressing temporal redundancies in the data through application of image optimal sampling, 2) addressing spatial redundancies in the data through cluster analysis, and 3) efficient coding of image data using standard still-image compression techniques.**

To illustrate the practicality of the proposed compression algorithm, a simulated positron emission tomography (PET) study using the fluoro-deoxy-glucose (FDG) tracer is presented. Realistic dynamic image data are generated by "virtual scanning" of a simulated brain phantom as a real PET scanner. These data are processed using the conventional [8] and proposed algorithms as well as the techniques for storage and analysis. The resulting parametric images obtained from the conventional and proposed approaches are subsequently compared to evaluate the proposed compression algorithm. As a result of this study, storage space for dynamic image data is able to be reduced by more than 95%, without loss in diagnostic quality. Therefore, the proposed theory and algorithm are expected to be very useful in medical image database management and telecommunication.

***Index Terms*—Cluster analysis, functional/parametric imaging, image compression, parameter estimation, positron emission tomography (PET), sampling schedule.**

I. Introduction

THE RECENT development in digital technology has opened new opportunities for advanced medical imaging. However, some medical imaging modalities acquire large volumes of data. For example, a positron emission tomography (PET) study using the CTI 951 scanner consists of 31 cross-sectional image planes, each of which has 128 × 128 pixels, acquired at multiple times to obtain a time-dependent, three-dimensional (3-D) characterization of the tissue tracer uptake. The resulting data set is, therefore, four-dimensional (4-D), consisting of approximately 11 million data points and requiring 22 megabytes of storage (for a typical 22 temporal-frame dynamic study) using the standard CTI-image format. With the advances in PET, imaging resolutions will continue to improve, further increasing the volume of associated data. This poses significant problems in terms of data storage, database management, retrieval, telecommunication, and processing. In order to reduce the amount of data needed to represent an image and help overcome some of these problems, various image compression algorithms may be used [1]. Image compression algorithms can be divided into two main categories, lossless and lossy compression algorithms. Lossless compression algorithms allow for perfect reconstruction of the original images from compressed data. These algorithms yield modest compression ratios (typically between 1.7 : 1 and 2.1 : 1 for medical image data [2]). To achieve higher compression ratios, lossy compression algorithms are required. Using lossy compression algorithms, the original images can only be reconstructed approximately from compressed data.

Various algorithms have been proposed for lossy compression of image data. The most popular algorithms are based on transform and subband coding [3]–[5], predictive coding [6], and vector quantization [2]. Transform and subband coding involve transformation of the input scalars or vectors by matrix operations or linear filtering. The most popular transform is the discrete cosine transform (DCT) [4]. This transform is used in the Joint Pictures Expert Group (JPEG) standard for still-image compression [7]. Many other transforms, such as Fourier, wavelet, and fractal transforms have recently been investigated [3], [5]. Predictive coding is based on linear prediction and involves a basic differential pulse-code modulation (DPCM) system. A scalar quantizer is used to quantize predication error formed by taking the difference between the input scalar and predicted input, based on previous inputs [6]. In the previous algorithms, pixels in an image are simply considered and compressed one at a time. The main idea behind vector quantization is to consider groups of pixels [2]. This allows quantizers to specifically minimize average distortions, given assumed code structures and exploit redundancies in the data. The challenges posed by medical imaging are the development of compression algorithms that are nearly lossless for diagnostic purposes, yet attain high compression ratios to reduce storage, transmission, and processing. In the case of dynamic image data, both spatial and temporal redundancies need to be considered. In general, the lossy compression algorithms mentioned above are not specifically tailored for dynamic

Manuscript received April 22, 1997; revised November 28, 1997. This work was supported by ARC and RGC grants.

D. Ho is with the Biomedical and Multimedia Information Technology (BMIT) Group, Basser Department of Computer Science, The University of Sydney, Sydney, 2006 Australia (e-mail: dinosaur@cs.usyd.edu.au).

D. Feng is with the Biomedical and Multimedia Information Technology (BMIT) Group, Basser Department of Computer Science, The University of Sydney, Sydney, 2006 Australia, and with Hong Kong Polytechnic University, Hung Hom, Kowloon, Hong Kong (e-mail: feng@cs.usyd.edu.au)

K. Chen is with the Samaritan PET Center, Phoenix, AZ 85006 USA.

Publisher Item Identifier S 1089-7771(97)09405-3.

image data. As a result, these algorithms are unable to fully exploit spatial and temporal redundancies in the data.

In this paper, we focus our attention to near (or diagnostically) lossless compression of dynamic image data. The theory developed is generally applicable to all types of imaging modalities in which dynamic image data is acquired, such as, PET and single-photon emission-computed tomography (SPECT) [8], [9]. To illustrate the practicality of this new compression algorithm, an example utilizing simulated PET-fluoro-deoxy-glucose (FDG) data is presented. The tracer FDG is an analogy of glucose and is used to study the metabolic rates of various tissue structures in the body. In this paper, the study was restricted to simulated data. Using computer simulation studies, the original, error-free parametric images are available for comparison. In evaluating the new compression algorithm, various image quality measures and quality testing issues are considered.

II. Functional/Parametric Imaging

Tracer kinetic techniques are widely used in PET to extract valuable information from dynamic processes in the body. This information is usually defined in terms of a mathematical model $\mu(\mathbf{t}|\mathbf{p})$ (where $\mathbf{t} = 1, 2, \cdots, T$ and $\mathbf{p}$ are the model parameters), whose parameters describe the delivery, transport, and biochemical transformation of the tracer. The driving function for the model is the plasma-blood input function, which is often obtained from blood sampling [8]. Measurements acquired by PET define the tissue time activity curve (TAC), or output function, denoted $z_i(\mathbf{t})$, where $\mathbf{t} = 1, 2, \cdots, T$ are discrete sampling times of the measurements and $i = 1, 2, \cdots, I$ corresponds to the ith pixel in the imaging region. The purpose of dynamic PET image analysis is to obtain tracer TAC's and parameter estimates $\hat{\mathbf{p}}$ for each pixel in the imaging region. These parameters may provide information of interest in themselves or may be used to define other physiological parameters, such as the metabolic rate of glucose (MRGlc) [8].

Fig. 1 shows the conventional steps involved in parametric image generation from the complete set of acquired PET projection data. Once the projection data is reconstructed, parameter estimation is performed on a pixel-by-pixel basis using certain rapid estimation algorithms [8], [10]–[12]. In this paper, we use the traditional-weighted nonlinear least-squares (WNLS) method purely for the purpose of comparing the estimation accuracy of the original and compressed data [8].

III. Compression Algorithm

The goal of a compression algorithm is to reduce the size of data required for storage, retrieval, and transmission and facilitate in analysis of the compressed data. To achieve this, efficient methods are required to exploit and code redundancies in the data. Fig. 2 gives an overview of the stages involved in the proposed compression algorithm.

- **Stage 1**: Exploit temporal redundancies in the data. Applying the image optimal-sampling schedule (OSS) design developed by the Biomedical and Multimedia Information Technology (BMIT) Group, The University of Sidney, Australia, [12], [13]. The number of temporal frames can be reduced while preserving data quality and fidelity (Section III-A).
- **Stage 2**: Exploit spatial redundancies in the data. Using cluster analysis, the reduced set of temporal frames can be further compressed to a single indexed image. This indexed image contains a mapping of the cluster groups for the reduced set of temporal frames and corresponds to the spatial information in the PET data. The respective temporal information for each cluster group is contained in an index table. This table is sequentially indexed by the cluster group, and each index contains the mean TAC cluster values for that group (Section III-B).
- **Stage 3**: Efficient coding of image data. Applying standard still-image compression techniques to the single indexed image, the dynamic data were further compressed (Section III-C).

For a detailed discussion of OSS and still-image compression techniques, refer to [12]–[14]. For the purpose of brevity, only the essential concepts are summarized below.

A. Stage 1: Compression in the Temporal Domain (OSS Design)

In PET studies, the reliability of the temporal frames is directly influenced by the sampling schedules and durations used to acquire the data. The longer the durations and greater the radioactivity counts, the more reliable the temporal frames. However, to obtain quantitative information from the dynamic processes, a certain number of temporal frames are required. Recently, the BMIT Group has shown that the minimum number of temporal frames required is equal to the number of model parameters to be estimated [12]. Based on this, an algorithm that automatically determines OSS and maximizes the information content of the acquired PET data was developed [13]. The developed algorithm utilizes the accumulated/integral PET measurements.

In the design of OSS, a new objective function based on the *Fisher Information Matrix* [15], [16] was proposed to limit the loss of dynamic information. This objective function was used to discriminate between different experimental protocols and sampling schedules. In this paper, we apply OSS to acquisition of PET projection data. This reduces the number of temporal frames obtained and, therefore, reduces data storage. Furthermore, as fewer temporal frames are reconstructed, the computational burden posed by image reconstruction is reduced. For a more detailed discussion on the theory and principles of OSS, refer to [12] and [13].

B. Stage 2: Compression in the Spatial Domain (Cluster Analysis)

Cluster analysis aims at grouping and classifying pixelwise TAC's $z_i(t)$ (where $i = 1, 2, \cdots, I$) into C_j cluster groups (where $j = 1, 2, \cdots, J$ and $J \ll I$) by natural association, according to self-similarity (or dissimilarity) characteristics. It is expected that TAC's with high degrees of natural association will belong to the same cluster groups, and conversely, TAC's

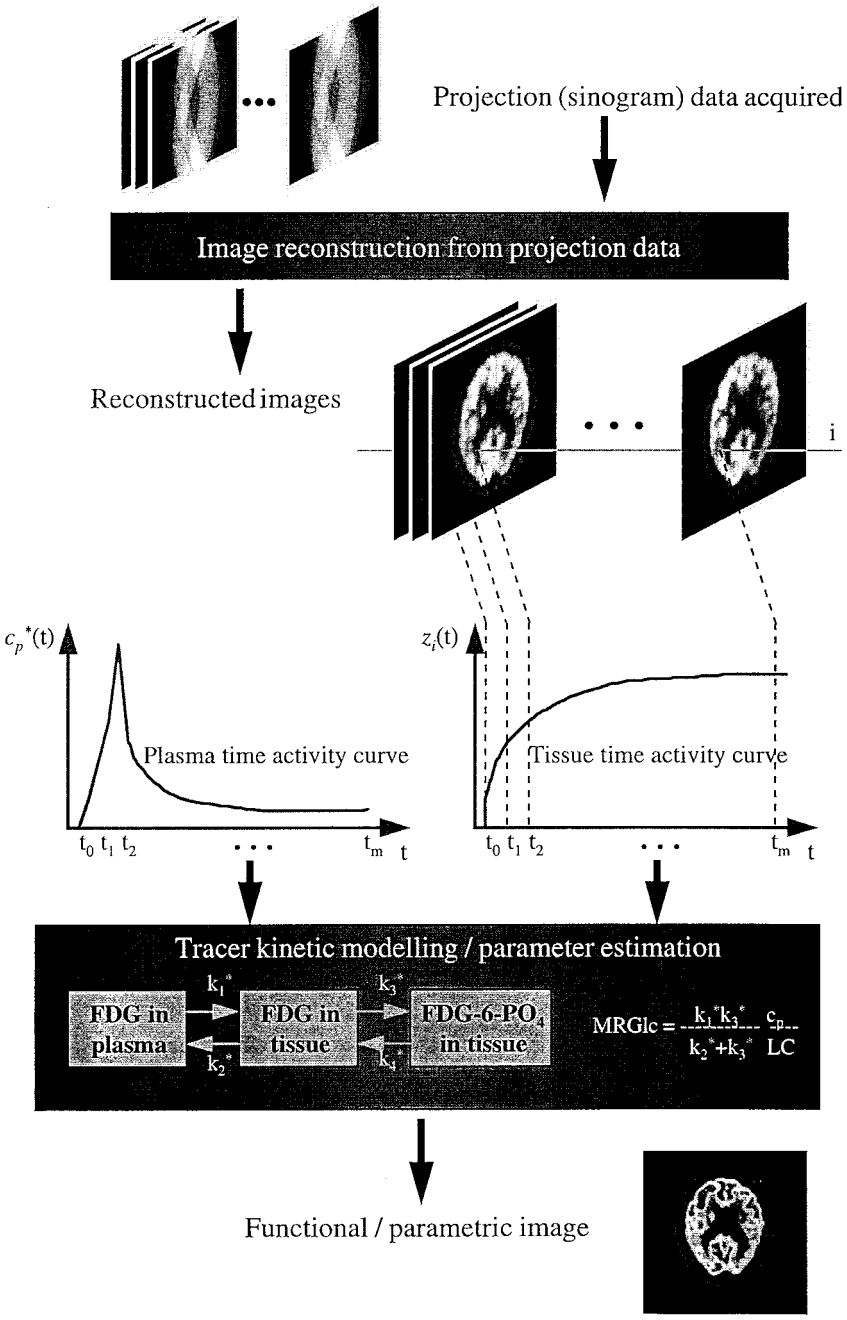

Fig. 1. Generation of parametric images using the conventional pixel-by-pixel analysis approach.

with low degrees will belong to different groups [17], [18]. For clustering to be valid, each TAC must be assigned uniquely to a cluster group (i.e., no TAC is allowed to belong to two different groups).

Many algorithms have been developed and used for clustering [17], [18]. They can be divided into direct (constructive) or indirect (optimization) algorithms, depending on whether a criterion measure is used during cluster analysis. The direct algorithms perform clustering without the necessity of a criterion measure, whereas indirect algorithms use the criterion measure to optimize clustering. Clustering algorithms can be further classified as agglomerative or divisive, according to whether classification is in a top–down or bottom–up direction. With agglomerative clustering, TAC's coalesce to the nearest cluster groups, according to a threshold in a bottom–up direction. Agglomerative algorithms are more versatile than divisive algorithms, as they can be used with both qualitative and quantitative data.

In this paper, we use an indirect agglomerative clustering algorithm based on the traditional Euclidean distance criterion measure to classify the computer simulated data [18]. Although this algorithm is simple compared to other algorithms, greater than 98% of the pixelwise TAC's are correctly classified and excellent classification of cluster groups are obtained. However, in general, the application of this algorithm to clinical data does not provide good classification of cluster groups. Depending on the quality of obtained clinical data, greater than 30% of the pixelwise TAC's may be misclassified.

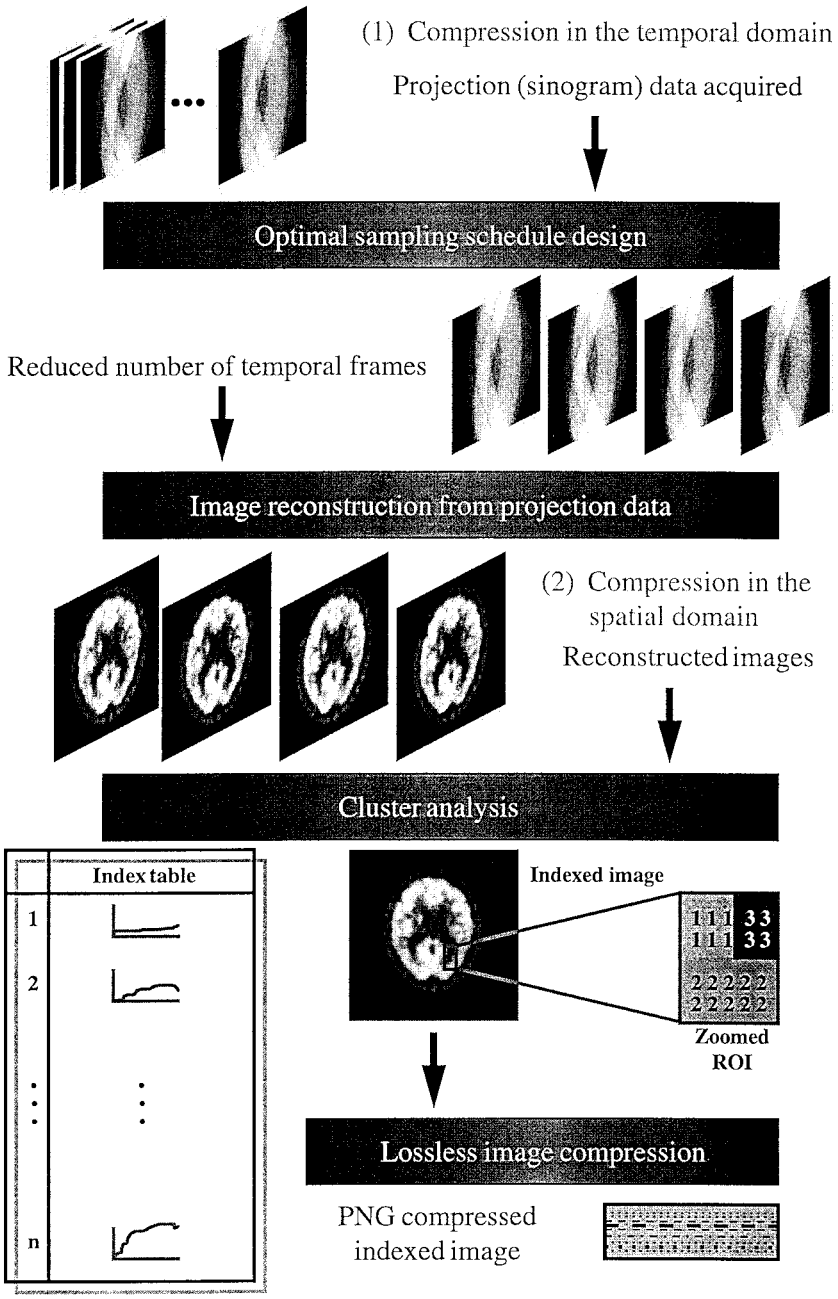

Fig. 2. Functional image data compression—Using the OSS theory, data redundancies in the acquired dynamic projection data are exploited. This results in data compression in the temporal domain. Cluster analysis and conventional still-image compression are used to further compress the dynamic image data in the spatial domain. The final compressed data includes an indexed image containing a mapping of the pixel TAC locations (compressed and stored in the Portable Network Graphics (PNG) file format) and a cluster index containing the mean TAC within each cluster.

This misclassification is due to the inherent noise in clinical data and the fact that TAC values over the whole image volume do not take a number of discrete values, but rather a continuum of values [19]. In this case, an interesting analogy with principal component and factor analysis may be made where similar considerations apply [20], [21]. For the purposes of this study, the clustering algorithm used is sufficient to cluster the simulated data. Several alternative algorithms for clustering of real clinical data are under investigation in our group. The results of these studies will be reported separately.

The Euclidean distance criterion measure used in the clustering algorithm is defined as

$$D^2(z_i, \overline{z}_{C_j}) = \sum_t (z_i(t) - \overline{z}_{c_j}(t))^2 \tag{1}$$

where $\overline{z}_{c_j}(t)$ (for $c_j = 1, 2, \cdots, J$) denotes the mean TAC within each cluster C_j.

Using the results of cluster analysis, an index table containing the mean TAC within each cluster group $\overline{z}_{c_j}(t)$ and an indexed image can be formed. The indexed image represents a mapping of the cluster groups to their respective pixel TAC

locations. This image, together with the index table, form the basis of the compressed temporal/spatial data. With PET, the number of distinguishable cluster groups will generally not exceed 64. This means that an 8-bit indexed image is sufficient to represent the cluster mapping.

C. Stage 3: Image Compression

Image compression addresses the problem of reducing the amount of data required to represent an image. A lossless compression scheme is considered in this paper for further reduction of the indexed image. In general, the underlying basis of the reduction process for lossless compression is efficient coding of image data by using as few bits as possible. From a mathematical point of view, this amounts to transforming the image into a statistically uncorrelated data set. Various coding techniques have been proposed for image compression [14]. In general, these techniques use predictive models or multiresolution image models to reduce statistical redundancies and encode residuals by using optimal encoders, such as Huffman [22], Lempel–Ziv (LZ) [23], or arithmetic coding [24].

In this paper, we compress and store the indexed image obtained from cluster analysis by using the Portable Network Graphics (PNG) file format [25]. The coding technique presently defined and implemented for PNG is based on deflate/inflate compression with a 32-kilobyte sliding window. Deflate compression is based on a LZ-77 derivate [23] and encoded by using fixed or custom Huffman codes. The PNG file format was chosen over other lossless image compression file formats due to its portability, flexibility, and being legally unencumbered. Furthermore, PNG supports a variety of features, such as indexed color images, greyscale images up to 16-bits/pixel, true color images up to 48-bits/pixel, transparency, gamma information, progressive display, and file-integrity checking. For a more detailed discussion of the PNG file format and its included features, refer to [25].

IV. Parametric Imaging Approach for Compressed Data

This approach uses the compressed data obtained from the proposed compression algorithm for the image analysis and subsequent generation of parametric images. In Fig. 3, the following various steps involved in generating parametric images from the compressed data are shown.

- **Step 1:** Decompression of indexed image. Since lossless compression is used for compressing the indexed image, a perfect reconstruction of the image is possible.
- **Step 2:** Tracer kinetic modeling and parameter estimation. Using the cluster TAC's defined in the index table, obtain parameter estimates for the tracer kinetic model by fitting $\overline{z}_{c_j}$ to the model equation $\mu(\mathbf{t}|\mathbf{p})$. Subsequently, calculate the physiological parameter of interest using the obtained estimates.
- **Step 3:** Pixelwise mapping. Map the obtained estimates and calculated physiological parameters for each cluster TAC to their respective pixel locations by referencing the indexed image. The resultant images correspond to the generated parametric images.

V. Numerical Evaluation and Performance Characteristics

A simulated brain PET study was carried out to examine performance characteristics of the proposed compression algorithm and the image quality of subsequent parametric images generated by image analysis. Using different tissue types, the computer-simulated phantom shown in Fig. 4(a) and the FDG model for brain studies, a dynamic PET brain phantom was generated. To reduce the memory requirements of the simulation study, only a single cross-sectional slice at an imaging resolution of 256 $\times$ 256 pixels with 16-bits/pixel was considered.

The well-known three-compartmental FDG model was used to define TAC's for various regions in the simulated phantom [8]. The differential equations governing this model are given by

$$\begin{aligned}\frac{d}{dt}c_e^*(t) &= k_1^* c_p^*(t) - (k_2^* + k_3^*)c_e^*(t) + k_4^* c_m^*(t)\\ \frac{d}{dt}c_m^*(t) &= k_3^* c_e^*(t) - k_4^* c_m^*(t)\end{aligned} \tag{2}$$

and the model function is given by

$$\mu(t|\mathbf{p}) = \mathbf{c_e^*(t)} + \mathbf{c_m^*(t)}$$

where $\mathbf{p}$ is the unknown vector of parameters to be estimated and $\mathbf{p} = (k_1^*, k_2^*, k_3^*, k_4^*)$. k_1^*–k_4^* are the rate constant parameters of the FDG model. $c_p^*(t)$, $c_e^*(t)$, and $c_m^*(t)$ correspond to the concentration of FDG in the plasma, FDG in the tissue, and phosphorylated FDG in the tissue, respectively. Once the unknown model parameters have been estimated, the physiological parameter for the metabolic rate of glucose (MRGlc) can be calculated as

$$\text{MRGlc} = \frac{1}{\text{LC}}\frac{k_1^* k_3^*}{k_2^* + k_3^*}c_p \tag{3}$$

where LC$(= 0.418)$ denotes the lumped constant that summarizes the difference between FDG and glucose in transportation and phosphorylation, and $c_p (= 91.9$ mg$/100$ ml$)$ corresponds to the "cold" glucose concentration in plasma [8]. The parameter values for various regions in the simulated phantom are obtained from real PET studies and correspond to tissue variations of grey, white, and whole matter [8]. c_p^*, the concentration of FDG in plasma, was obtained from human studies [11]. The sampling durations for the measurement of the PET data using the conventional pixel-by-pixel analysis approach are consistent with the conventional sampling schedule (CSS) for routine FDG studies. The OSS proposed by Li *et al.* [13] was used for generating projection data for the compressed data analysis approach. The sampling times for CSS are given by 0.2, 0.4, 0.6, 0.8, 1.0, 1.2, 1.4, 1.6, 1.8, 2.0, 2.5, 3.0, 4.0, 5.0, 6.5, 10.0, 15.0, 20.0, 30.0, 60.0, 90.0, and 120.0 min and for OSS are given by 2.733, 15.683, 77.066, and 120.0 min [13]. These sampling times are the starting-time points of the dynamic image frames, except the last sampling time, which is the end point of the last frame.

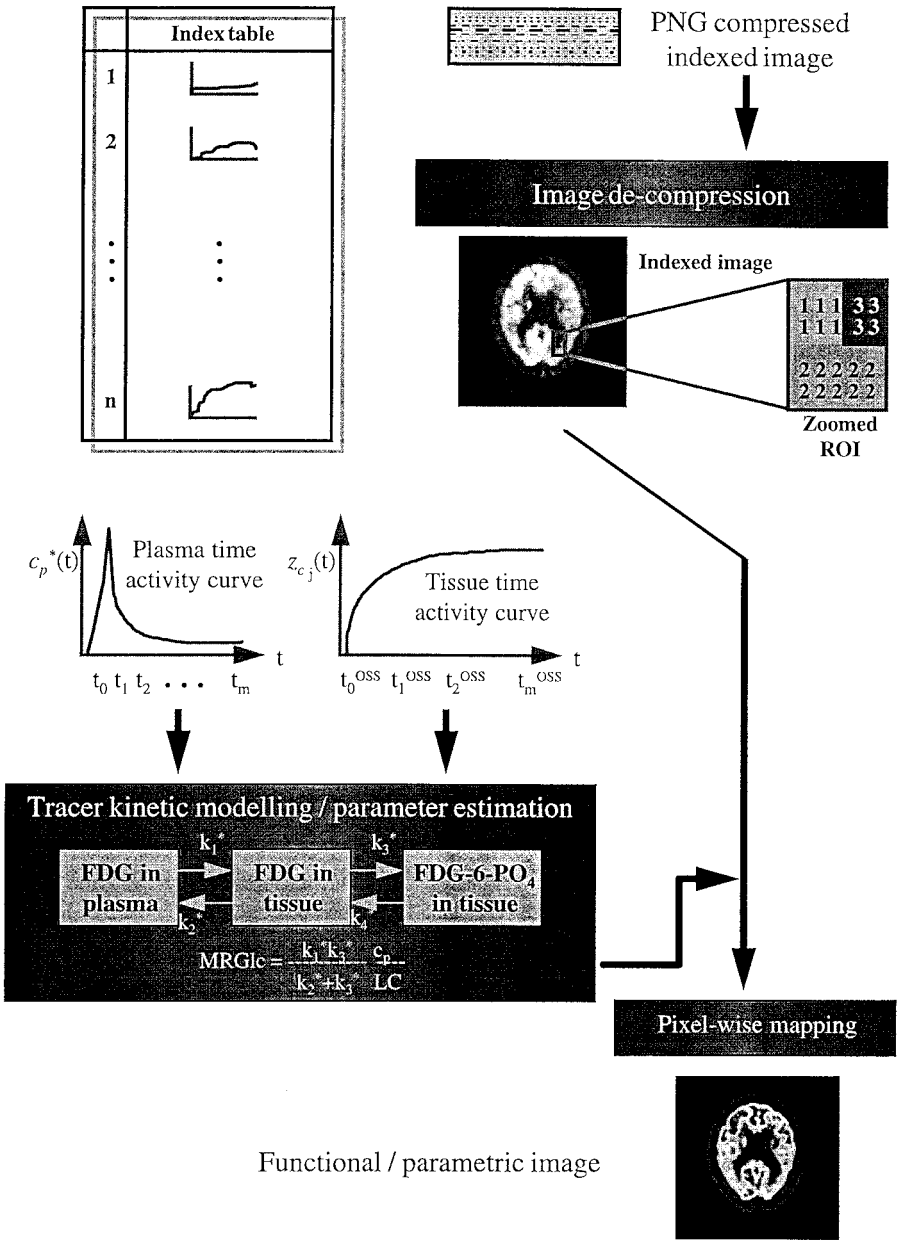

Fig. 3. Generation of parametric images based on the compressed data.

By virtual scanning of the dynamic brain phantom as a real PET scanner, dynamic PET projection data were obtained. To simulate realistic PET measurement noise, an additive noise contribution following a Poisson distribution was imposed on the simulated PET projection measurements by using CSS (a pseudorandom number generator was used). Noise corresponding to a 20–90% deviation in the first ten PET measurements (represents a 2% deviation in the last PET measurement) was applied. This noise level is comparable to that expected in real clinical data. The noisy, simulated PET projection data were reconstructed by using the popular, filtered back-projection algorithm, with normal parameter values used in routine procedures. The Generalized Hamming filter, with a Hamming distance $\alpha = 0.5$, was used in this study [26]. To evaluate the compression procedure, the reconstructed dynamic image data were used.

In this paper, the study was restricted to simulated data. This allows us to compare and evaluate the quality of the generated parametric images obtained from the conventional pixel-by-pixel analysis approach by using the complete set of data (Fig. 1) and the proposed compressed data analysis approach (Fig. 3), with the original, error-free parametric images.

A. Compression Measures

Various measures have been used for reporting and comparing compression results [27]. The most commonly used measures include the compression ratio (CR $= t/l$, where t is the original file size and l is the compressed file size, e.g., 2.0 : 1) and relative compression (RC $= (t - l)/t \times 100\%$, e.g., 50.0%). In this paper, we use these measures and include an additional measure, percent compression gain

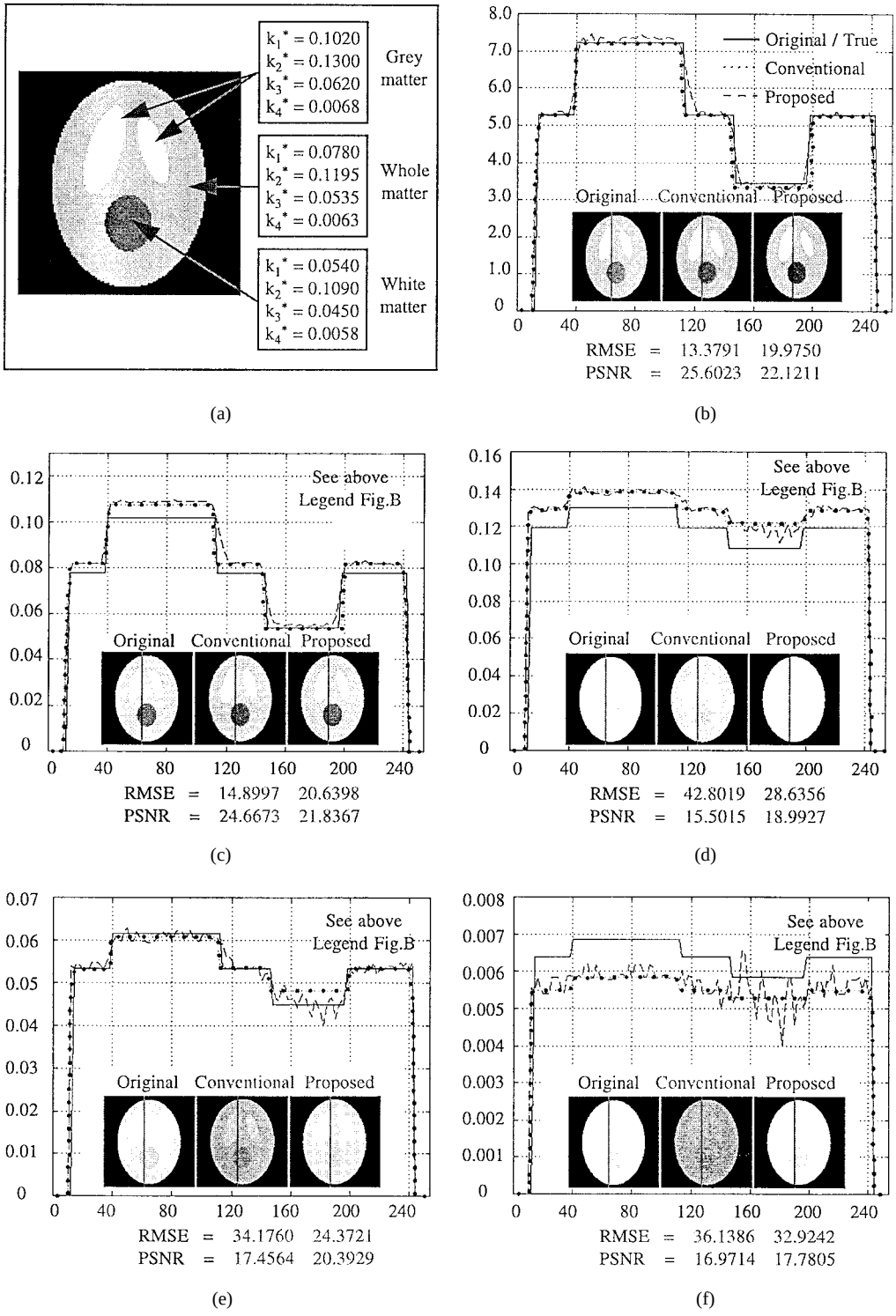

Fig. 4. (a) Dynamic phantom used in the simulation study for generating dynamic PET projection data. The FDG model was used to define TAC's for various regions in the phantom. Rate constants corresponding to various tissue types are used, for grey matter: $k_1^* = 0.1020$, $k_2^* = 0.1300$, $k_3^* = 0.0620$, and $k_4^* = 0.0068$; for white matter: $k_1^* = 0.0540$, $k_2^* = 0.1090$, $k_3^* = 0.0450$, and $k_4^* = 0.0058$; and for whole matter: $k_1^* = 0.0780$, $k_2^* = 0.1195$, $k_3^* = 0.0535$, and $k_4^* = 0.0063$. (b)–(f) Vertical profiles for the generated parametric images. The solid lines correspond to profiles obtained from the original, error-free parametric images, the dashed lines correspond to the conventional pixel-by-pixel image analysis approach, and the dotted lines correspond to the proposed compressed-data image analysis approach. RMSE and PSNR correspond to the root mean square error and the peak signal-to-noise ratio, respectively.

(CG $= 100\ln(t/l)$, where ln is the natural logarithm, e.g., 69.3%) [27]. CG has several additional advantages over the commonly used measures (CR and RC). First, this measure does not express compression relative to the original file and, therefore, can be used as a measure, with respect to any standard. Second, CG is additive and allows us to simply add together effects of multiple cascaded compressors. For a more detailed discussion on CG, refer to [27].

TABLE I
COMPRESSION RESULTS FOR A TYPICAL PET STUDY AT AN IMAGING RESOLUTION OF 256 × 256 AND A SINGLE CROSS-SECTIONAL PLANE. THE CSS OF 22 TEMPORAL FRAMES WAS USED. TWO BYTES ARE REQUIRED TO REPRESENT EACH PIXEL IN THE TEMPORAL FRAMES

Complete data (22 time frames CSS)	$256 \times 256 \times 22 \times 2$
	$= 2,883,584$ bytes
CR = 1.0:1, CG = 0.0% and RC = 0.0%	
Stage 1: Compression in the temporal domain	$256 \times 256 \times 4 \times 2$
optimal sampling schedule (4 time frames OSS)	$= 524,288$ bytes
CR = 5.5:1, CG = 170.47% and RC = 81.8%	
Stage 2: Compression in the spatial domain - cluster analysis	
Assume a maximum of 256 different clusters	
(based on the 8-bit indexed image)	
i) indexed image	$256 \times 256 \times 1$
	$= 65,536$ bytes
ii) cluster index	$256 \times 4 \times 2$
	$= 2048$ bytes
	total size $= 67,584$ bytes
CR = 7.8:1, CG = 204.87% and RC = 87.1%	
Stage 3: Conventional image compression (data dependent)	
PNG still-image compression	assume CR = 2.0:1
(lossless compression algorithm)	typical for medical
	images
i) indexed image	$= 32,768$ bytes
ii) cluster index	$= 2048$ bytes
	total size $= 34,816$ bytes
CR = 1.9:1, CG = 66.33% and RC = 48.5%	
Overall: CR = 82.8:1, CG = 441.67% and RC = 98.8%	

B. Image Quality Measures

For any lossy compression algorithm, a measure is required to evaluate the image quality and fidelity after decompression of the compressed data. In the case of PET, we require parametric images obtained after image analysis of the compressed data to have equivalent qualitative and quantitative quality as images obtained after analysis of the complete set of acquired PET projection data. In this paper, the root mean square error (RMSE) and the peak signal-to-noise ratio (PSNR) measures are considered. RMSE is evaluated as

$$\text{RMSE} = \sqrt{\frac{1}{I}\sum_{x=1}^{I}\left\{f_i - \tilde{f}_i\right\}^2} \tag{4}$$

where I corresponds to the number of pixels in the image, f_i is the value of the ith pixel in the original, error-free parametric image, and $\tilde{f}_i$ is the value of the ith pixel in the parametric image, based on the image analysis of the complete or compressed data. The PSNR is a measure of image fidelity, its units are in decibels (dB). It is defined as

$$\text{PSNR} = -20\log_{10}\left(\frac{\text{RMSE}}{2^n - 1}\right) \tag{5}$$

where n is the number of bits/pixel in the image.

VI. RESULT/DISCUSSION

In Table I, results for each stage of the compression algorithm for a typical PET study are shown. OSS was used to compress the dynamic projection data in the temporal domain, and a CR of 5.5 : 1 was obtained. Using cluster analysis, the reconstructed images were further compressed in the spatial domain, obtaining a CR of 7.8 : 1. Finally, the indexed image obtained from cluster analysis was compressed and stored by using the PNG file format. A typical CR of 2.0 : 1 for medical images can be obtained for lossless still-image compression schemes [2], [27]. The global CR obtained for the proposed compression algorithm was 82.8 : 1. This CR corresponds to a CG of 441.67% and a RC of 98.8%.

The most important measure of a lossy compression algorithm is the resultant image quality and fidelity. Parametric images of MRGlc k_1^*, k_2^*, k_3^*, and k_4^*, generated after image analysis of the complete and compressed data are shown together with the original, error-free images in Fig. 4(b)–(f). The corresponding results for RMSE and PSNR, are shown in each figure. RMSE and PSNR obtained from the complete set of projection data and the compressed data are in agreement. Furthermore, images for k_2^*, k_3^*, and k_4^* obtained from the proposed compressed-data analysis approach have lower RMSE values and higher PSNR values than those obtained from the conventional pixel-by-pixel image analysis approach.

TABLE II
PARAMETRIC-IMAGE PHYSIOLOGICAL PARAMETER VALUES: SIMULATED PHANTOM

Region	MRGlc	k_1^*	k_2^*	k_3^*	k_4^*
True parameter values					
Background	0.0000	0.0000	0.0000	0.0000	0.0000
Region 1 (Whole)	5.3032	0.0780	0.1195	0.0535	0.0063
Region 2 (White)	3.4692	0.0540	0.1090	0.0450	0.0058
Region 3 (Grey)	7.2415	0.1020	0.1300	0.0620	0.0068
Image analysis of complete projection data					
Conventional pixel-by-pixel analysis approach					
Background	0.0000	0.0000	0.0000	0.0000	0.0000
Region 1 (mean)	5.2524	0.0813	0.1291	0.0536	0.0056
(Whole) (stddev)	0.3246	0.0048	0.0013	0.0010	0.0002
Region 2 (mean)	3.3639	0.0548	0.1177	0.0453	0.0052
(White) (stddev)	0.0590	0.0004	0.0013	0.0013	0.0005
Region 3 (mean)	7.2590	0.1083	0.1383	0.0607	0.0059
(Grey) (stddev)	0.1476	0.0018	0.0010	0.0008	0.0001
Image analysis of compressed data					
Proposed compressed data analysis approach					
Background	0.0000	0.0000	0.0000	0.0000	0.0000
Region 1 (Whole)	5.3061	0.0822	0.1298	0.0539	0.0056
Region 2 (White)	3.3710	0.0541	0.1224	0.0484	0.0054
Region 3 (Grey)	7.2508	0.1081	0.1391	0.0611	0.0060

In Fig. 4(d)–(f), it is easy to see that higher PSNR's obtained for k_2^*, k_3^*, and k_4^* from the proposed approach correspond to *sharper* defined images in comparison to images obtained from the conventional pixel-by-pixel image analysis approach.

The results shown so far have highlighted the qualitative quality of parametric images obtained from the conventional pixel-by-pixel and the proposed compressed-data image analysis approaches. With PET, quantitative quality of the obtained parametric images is of equal, if not more, importance. In Table II, extracted parameters for MRGlc k_1^*, k_2^*, k_3^*, and k_4^* from the generated parametric images for various regions in the simulated phantom are shown. The number of pixels included in the various regions were 34 376 pixels for the background, 24 148 pixels in region 1, 2368 pixels in region 2, and 4644 pixels in region 3. For the conventional image analysis approach, values of 7.2590, 3.3639, and 5.2524 mg/min/100 ml for grey, white, and whole matter, respectively, were obtained. For the proposed compressed-data analysis approach, values of 7.2508, 3.3710, and 5.3061 mg/min/100 ml for grey, white, and whole matter, respectively, were obtained. The values obtained from the conventional and proposed approaches were in agreement with the expected values of 7.2415, 3.4692, and 5.3032 mg/min/100 ml. Similarly, the estimated rate constant values for k_1^*, k_2^*, k_3^*, and k_4^* obtained using the conventional and proposed approaches were in agreement with the theoretically expected values, as listed in Table II.

In Fig. 4(b)–(f), vertical profiles for the generated parametric images are also shown. The solid lines in the figures correspond to profiles obtained from the original, error-free parametric images, the dashed lines correspond to the conventional pixel-by-pixel image analysis approach, and the dotted lines correspond to the proposed compressed-data image-analysis approach. It is easy to see that parametric images generated using the conventional image analysis approach contain a certain amount of noise (in particular, images for k_2^*, k_3^*, and k_4^*). This noise is due to reconstruction of the projection data [28]. In the case of the proposed compressed-data image-analysis approach, the cluster analysis acts as an averaging filter and significantly reduces noise in the generated parametric images.

For generation of parametric images, the major computations involved are the curve fittings of TAC's. Since the number of TAC's required to be fit using the compressed data are significantly smaller, the proposed image analysis approach is significantly faster than the conventional pixel-by-pixel image analysis approach. If we neglect background pixels, over 31 160 curve fittings are required, based on the conventional pixel-by-pixel image analysis approach. With the proposed image analysis approach, the number of curve fittings required is determined by the number of TAC's in the index table. Therefore, in the worst-case scenario, 256 curve fittings are required (based on an 8-bit indexed image). For the simulated data, only three curve fittings were performed based on the proposed image analysis approach.

In addition to image analysis, the computational time required for compressing the complete acquired PET projection data needs to be considered. In this study, we found that the additional overhead contributed due to the compression algorithm did not increase computational complexity. The overhead due to cluster analysis and image compression were accounted for in the OSS stage. Using OSS, only four temporal frames were reconstructed, in comparison to the 22 temporal frames required by CSS, using the conventional image analysis approach.

VII. CONCLUSION

In this paper, a near (or diagnostically) lossless algorithm for dynamic image data compression was proposed and systematically evaluated. In order to fully exploit data redundancies in the acquired dynamic data, domain-specific knowledge related to medical imaging, the medical practice and the dynamic imaging modality are incorporated into the compression scheme. Redundancies in the data in both the temporal and spatial domain are exploited. The results showed that the proposed algorithm was able to reduce required storage space by more than 95%, without loss in diagnostic quality, and greatly reduced the computational complexity for further image analysis and generation of parametric images. Therefore, the proposed algorithm for dynamic image data compression is expected to be very useful in medical-image data management and telecommunication.

REFERENCES

[1] M. Nelson and J. L. Gailly, *The Data Compression Book*, 2nd ed. New York: M & T Books, 1996.

[2] R. M. Gray, P. C. Cosman, and E. A. Riskin, "Image compression and tree-structure vector quantization," in *Image and Text Compression,* J. Storer, Ed. Norwell, MA: Kluwer, 1992, pp. 3–34.
[3] Y. Fisher, B. Jacobs, and R. Boss, "Fractal image compression using iterated transforms," in *Image and Text Compression,* J. Storer, Ed. Norwell, MA: Kluwer, 1992, pp. 35–61.
[4] H. Lee, Y. Kim, A. H. Rowberg, and E. A. Riskin, "Statistical distributions of dct coefficients and their applications to an interframe compression algorithm for 3-D medical images," *IEEE Trans. Med. Imag.,* vol. 12, pp. 478–485, Sept. 1993.
[5] J. D. Villasenor, "Alternatives to the discrete cosine transform for irreversible tomographic image compression," *IEEE Trans. Med. Imag.,* vol. 12, pp. 803–811, Dec. 1993.
[6] K. Chen and T. V. Ramabadran, "Near-lossless compression of medical images through entropy-coded dpcm," *IEEE Trans. Med. Imag.,* vol. 13, pp. 538–548, Sept. 1994.
[7] G. K. Wallace, "The JPEG still picture compression standard," *Commun. ACM,* vol. 34, pp. 30–44, 1991.
[8] S. C. Huang, M. E. Phelps, E. J. Hoffman, K. Sideris, C. Selin, and D. E. Kuhl, "Noninvasive determination of local cerebral metabolic rate of glucose in man," *Amer. J. Physiol.,* vol. 238, pp. E69–E82, 1980.
[9] C. H. Lau, D. Feng, D. P. K Lun, and W.-C. Siu, "Dynamic imaging and modeling using a single-head rotating camera," submitted for publication.
[10] C. S. Patlak, R. G. Blasberg, and J. Fenstermacher, "Graphical evaluation of blood to brain transfer constants from multiple-time uptake data," *J. Cerebral Blood Flow Metabolism,* vol. 3, pp. 1–7, 1983.
[11] D. Feng, S. C. Huang, Z. Wang, and D. Ho, "An unbiased parametric imaging algorithm for nonuniformly sampled biomedical system parameter estimation," *IEEE Trans. Med. Imag.,* vol. 15, pp. 512–518, Aug. 1996.
[12] D. Feng, X. Li, and W. C. Siu, "A new dimension in image data compression: Theory and principles for the minimization of image frames in dynamic biomedical function imaging," *IEEE Trans. Nucl. Sci.,* to be published.
[13] X. Li, D. Feng, and K. Chen, "Optimal image sampling schedule: A new effective way to reduce dynamic image storage space and functional image processing time," *IEEE Trans. Med. Imag.,* vol. 15, pp. 710–718, Oct. 1996.
[14] A. K. Jain, "Image data compression: A review," in *Proc. IEEE,* vol. 69, pp. 349–389, 1981.
[15] D. Z. D'Argenio, "Optimal sampling times for pharmacokinetic experiments," *J. Pharm. Biopharm.,* vol. 9, pp. 739–756, 1981.
[16] C. Cobelli and A. Ruggeri, "Optimal design of sampling schedule for studying glucose kinetics with tracers," *Amer. J. Physiol.,* vol. 257, pp. E444–E450, 1989.
[17] S. T. Bow, *Pattern Recognition: Applications to Large Data-Set Problems.* New York: Marcel Dekker, 1984.
[18] E. J. Ciaccio, S. M. Dunn, and M. Akay, "Biosignal pattern recognition and interpretation systems: Methods of classification," *IEEE Eng. Med. Biol.,* vol. 13, pp. 129–135, 1994.
[19] J. Ashburner, J. Haslam, C. Taylor, V. J. Cunningham, and T. Jones, "A cluster analysis approach for the characterization of dynamic PET data," in *Quantification of Brain Function Using PET.* New York: Academic, 1996, pp. 301–306.
[20] T. Kao, S. H. Shieh, and L. C. Wu, "Dynamic radionuclide images compression based on principal components analysis," *1995 IEEE Eng. Med. Biol.,* pp. 1227–1228.
[21] H. M. Wu, C. K. Hoh, Y. Choi, H. R. Schelbert, R. A. Hawkins, M. E. Phelps, and S. C. Huang, "Factor analysis for extraction of blood time activity curve (TAC) in dynamic PET FDG studies," *J. Nucl. Med.* vol. 35, p. 71P, 1994.
[22] R. G. Galleger, "Variations on a theme by Huffman," *IEEE Trans. Inform. Theory,* vol. IT-24, pp. 668–674, Nov. 1978.
[23] A. Lempel and J. Ziv, "Compression of two-dimensional images," in *Combinatorial Algorithms on Words.* New York: Springer-Verlag, 1985, pp. 141–154.
[24] I. H. Witten, R. M. Neal, and J. G. Cleary, "Arithmetic coding for data compression," *Commun. ACM,* vol. 30, pp. 520–540, 1987.
[25] L. D. Crocker, "PNG: The portable network graphic format," *Dr. Dobb's J.,* pp. 36–49, July 1995.
[26] A. K. Jain, "Image reconstruction from projections," in *Fundamentals of Digital Image Processing.* Englewood Cliffs, NJ: Prentice-Hall, 1989, pp. 431–475.
[27] P. G. Howard and J. S. Vitter, "New methods for lossless image compression using arithmetic coding," *Inf. Process. Manage.* vol. 28, pp. 765–779, 1992.
[28] J. Doll, H. J. Ostertag, M. E. Bellemann, P. Schmidlin, W. K. Kubler, L. G. Strauss, and W. J. Lorenz, "Effects of distorted PET projection data on the reconstructed image using different reconstruction algorithms," in *Radioactive Isotopes in Clinical Medicine and Research Advances in Pharmacological Sciences.* Berlin, Germany: Birkhauser-Verlag, 1995, pp. 85–90.

Dino Ho received the B.S. (honors) and Ph.D. degrees in computer science in 1992 and 1997, respectively, both from The University of Sydney, Sidney, Australia.

He is with AT&T as an Associate in the Solutions Asia/Pacific network integration practice, Hong Kong, and with the Biomedical and Multimedia Information Technology (BMIT) Group, Basser Department of Computer Science, The University of Sydney. His current research interests include PET kinetic modeling, functional image/data compression, medical database systems, and telemedicine.

Dagan Feng (S'88–M'88–SM'94) received the Ph.D. degree in computer science from the University of California, Los Angeles, in 1988.

After briefly working as Assistant Professor at the University of California, Riverside, he joined The University of Sydney, Sidney, Australia, at the end of 1988 as a Lecturer, Senior Lecturer, and then Reader. He is currently a Professor at Hong Kong Polytechnic University, Hung Hom, and Founder and Director of the Biomedical and Multimedia Information Technology (BMIT) Group, The University of Sydney.

Dr. Feng is Vice-Chair of IFAC Technical Committee on BIOMED.

Kewei Chen received the B.S. and M.S. degrees in mathematics in 1982 and 1986, respectively, from Beijing Normal University, Beijing, China. He received the biomathematics Ph.D. degree from the University of California, Los Angles, in 1993.

He is currently a PET Biomathematician at Samaritan PET Center, Phoenix, AZ. His current research interests include PET kinetic modeling, statistical data analysis in PET brain activation studies, and Alzheimer studies.